

Flushing of the deep Pacific Ocean and the deglacial rise of atmospheric CO₂ concentrations

Jianghui Du^{1*}, Brian A. Haley¹, Alan C. Mix¹, Maureen H. Walczak¹ and Summer K. Praetorius²

During the last deglaciation (19,000–9,000 years ago), atmospheric CO₂ increased by about 80 ppm. Understanding the mechanisms responsible for this change is a central theme of palaeoclimatology, relevant for predicting future CO₂ transfers in a warming world. Deglacial CO₂ rise hypothetically tapped an accumulated deep Pacific carbon reservoir, but the processes remain elusive as they are underconstrained by existing tracers. Here we report high-resolution authigenic neodymium isotope data in North Pacific sediment cores and infer abyssal Pacific overturning weaker than today during the Last Glacial Maximum but intermittently stronger during steps of deglacial CO₂ rise. Radiocarbon evidence suggestive of relatively ‘old’ deglacial deep Pacific water is reinterpreted here as an increase in preformed ¹⁴C age of subsurface waters sourced near Antarctica, consistent with movement of aged carbon out of the deep ocean and release of CO₂ to the atmosphere during the abyssal flushing events. The timing of neodymium isotope changes suggests that deglacial acceleration of Pacific abyssal circulation tracked Southern Hemisphere warming, sea-ice retreat and increase of mean ocean temperature. The inferred magnitude of circulation changes is consistent with deep Pacific flushing as a significant, and perhaps dominant, control of the deglacial rise of atmospheric CO₂.

What role did abyssal circulation play in releasing carbon from the deep ocean to the atmosphere during the last deglaciation? Changes of water-mass boundaries have been reported based on stable isotopes^{1,2}, but palaeo-water-mass geometry does not necessarily constrain circulation rates^{3,4}. Radiocarbon is similarly inconclusive about rates^{5–13}. At face value, the presence of ¹⁴C-deficient deep waters during the deglaciation may suggest slow abyssal circulation^{12,13} and argues against carbon release from the deep Pacific. The use of ¹⁴C as a circulation rate tracer, however, is complicated by the influence of preformed ¹⁴C age³, which depends on air–sea carbon isotope exchange, which has a much longer equilibration timescale than gas exchange (years versus months)¹⁴. In the modern deep Pacific, the preformed age of Southern Ocean source water accounts for nearly half of the apparent water-mass ¹⁴C age¹⁵ (that is, the circulation age is much less than the ¹⁴C age), and it probably changed during the deglaciation^{13,16,17}.

The neodymium isotope composition (ϵ_{Nd}) of authigenic phases in marine sediments offers an independent constraint on Pacific circulation rates. We adopt a model in which the ϵ_{Nd} and the Nd budgets of the Pacific are significantly influenced by benthic fluxes^{18–21} (at all depths, but primarily from >3,000 m because of hypsometry, Methods, Supplementary Fig. 1). On the timescales of Pacific mixing, under this premise spatial and temporal changes in ϵ_{Nd} are modulated mostly by the non-conservative effect of sediment exposure time as a function of bottom water residence time^{19–21} (Methods). Such a model for modern deep Pacific ϵ_{Nd} is supported by the strong correlation between core-top authigenic ϵ_{Nd} and circulation age²² (Fig. 1, Supplementary Fig. 2).

We propose that to first order the Pacific benthic Nd flux has been approximately constant since the Last Glacial Maximum (LGM), because (1) over this timespan deep-sea sediment provenance changed little on the basinal scale and (2) benthic Nd flux is insensitive to changes in diagenetic redox regimes (Supplementary Methods, Supplementary Fig. 1). A consequence of this supposition is that temporal changes in authigenic ϵ_{Nd} in Pacific sediment cores

far from the water-mass source would be most strongly influenced by the abyssal circulation rate, wherein longer integrated sediment exposure time yields more radiogenic (higher) ϵ_{Nd} ^{19,20}.

Here we reconstruct deglacial Pacific circulation using two new, high-resolution (~200 yr deglacial sample interval) authigenic ϵ_{Nd} records from the Gulf of Alaska (Fig. 1). The deeper core EW0408-87JC and its reoccupation IODP site U1418 (58.8° N, 144.5° W, 3,680 m) underlie Pacific Deep Water (PDW), the ‘oldest’, most carbon-rich and for ϵ_{Nd} the most radiogenic water mass in the ocean today. This site is ideally located to record the integrated exposure time associated with the transit of Antarctic Bottom Water (AABW) across the full meridional span of the Pacific from south to north. The shallower core EW0408-85TC/JC and co-located IODP site U1419 (59.6° N, 144.2° W, 682 m) underlie North Pacific Intermediate Water (NPIW) at a depth less sensitive to abyssal overturning but potentially sensitive to interior stratification and formation of local North Pacific water masses.

We generated authigenic ϵ_{Nd} records by leaching non-decarbonated bulk sediments (Methods, Supplementary Fig. 3), and compared these data with the benthic–planktonic ¹⁴C age differences analysed from the same cores⁹ (Methods). Through a twin-tracer approach, we constrain abyssal circulation rate using ϵ_{Nd} , and deconvolve the preformed component of ¹⁴C age from water-mass age (Methods, Supplementary Methods). Because the adjustment timescales of both tracers are comparable to the timescales of deglacial climate change, understanding their temporal evolution necessitates a transient modelling approach³, which we employ here to constrain circulation history, and by comparison to sensitivity tests with detailed biogeochemical climate models to discuss its implications for the carbon cycle.

Deglacial evolution of North Pacific ϵ_{Nd}

Values of ϵ_{Nd} at the deep site were higher during the LGM than today (Fig. 2b), suggesting reduced AABW transport into the Pacific, in agreement with some model simulations²³. This sluggish circulation

¹College of Earth, Ocean and Atmospheric Sciences, Oregon State University, Corvallis, OR, USA. ²United States Geological Survey, Menlo Park, CA, USA. *e-mail: dujia@oregonstate.edu

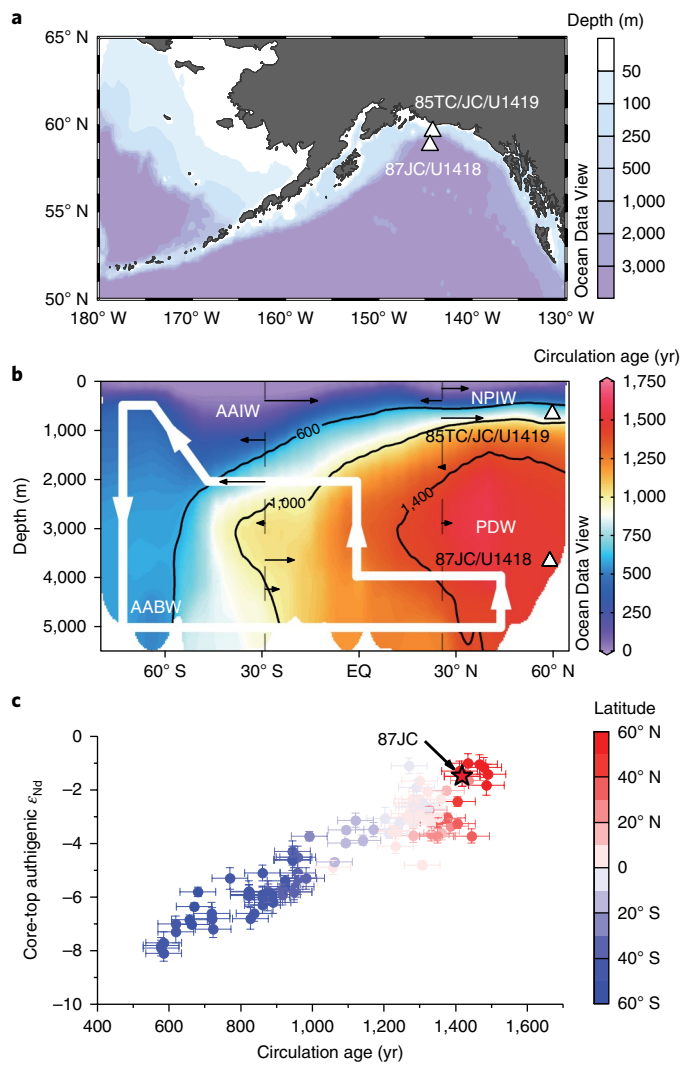


Fig. 1 | Study sites and Pacific circulation. **a**, Locations of the intermediate-depth (EW0408-85TC/JC/U1419) and the deep (EW0408-87JC/U1418) sites in the Gulf of Alaska. **b**, A meridional (138° W) section of circulation age in the Pacific²². Solid small arrows indicate modern water transport across the 28° S and 24° N hydrographic sections and thick arrows show the schematic abyssal circulation³⁴. **c**, Relationship between Pacific core-top authigenic ϵ_{Nd} (>2,500 m, Supplementary Fig. 2, with 2σ analytical uncertainty) and circulation age ($1\sigma = 50$ yr)²². The star symbol is site EW0408-87JC.

would have allowed accumulation of respired carbon in the glacial deep Pacific¹.

Deglacial decrease of our deep site ϵ_{Nd} (Fig. 2b) can be explained by faster overturning (less benthic exposure time). The change in ϵ_{Nd} near 19 ka (thousand years ago) coincides with the initial deglacial warming of West Antarctica²⁴, reduction of Antarctic sea ice (indicated by decreasing sea-salt sodium concentration)²⁵ and the first significant postglacial sea-level rise²⁶, but predates the sustained warming of East Antarctica²⁷ and the rapid atmospheric CO_2 increase²⁸ (Fig. 2). After this early change, further ϵ_{Nd} decrease corresponds to steps of atmospheric CO_2 rise between 18–14.5 ka and 13–11.5 ka, during which times sea ice retreated and temperature increased synchronously in West and East Antarctica together with the global ocean²⁹. These intervals also saw negative atmospheric $\delta^{13}C$ excursions^{30,31} and reduced Southern Ocean stratification^{1,8,13,16,32,33} (Fig. 2d,e). All these signals are consistent with

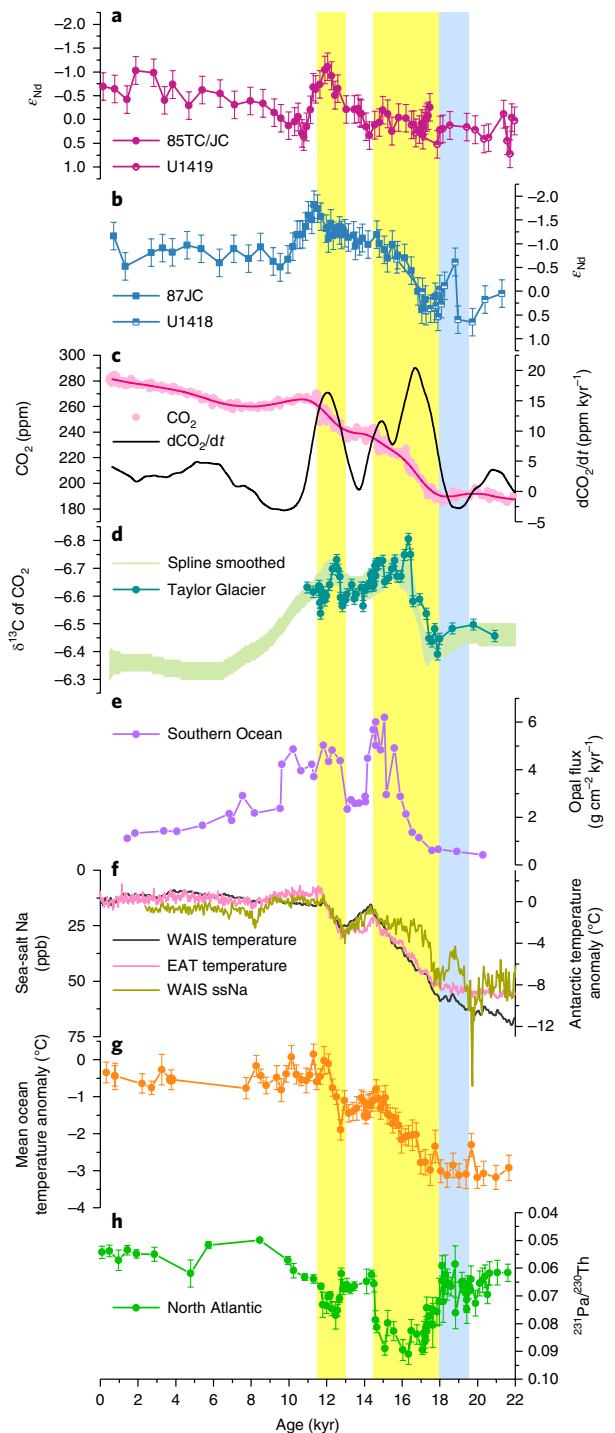


Fig. 2 | Deglacial North Pacific ϵ_{Nd} compared with global climate records.

a, b, Authigenic ϵ_{Nd} from site EW0408-85TC/JC/U1419 (**a**) and site EW0408-87JC/U1418 (**b**). Error bars in **a** and **b** indicate long-term 2σ (0.29 ϵ) external reproducibility (Methods). **c**, Ice-core CO_2 and its rate of change^{28,55}. **d**, $\delta^{13}C$ of atmospheric CO_2 ^{30,31}. **e**, Southern Ocean opal flux from core TN057-13PC4³². **f**, Temperature anomalies from West (WAIS Divide)²⁴ and East (EAT)²⁷ Antarctica, and sea-salt sodium concentration (ssNa, 50-year median value, a proxy for sea ice) from the WAIS Divide²⁵. **g**, Mean ocean temperature anomaly with 1σ uncertainty²⁹. **h**, North Atlantic $^{231}Pa/^{230}Th$ records with 1σ uncertainty^{45,56}. The blue-shaded interval marks the early deglacial increase of temperature and decrease of sea ice in West Antarctica. The yellow-shaded intervals mark the synchronous increase of atmospheric CO_2 , decrease of sea ice and increase of temperature in both West and East Antarctica, and rise of global ocean mean temperature.

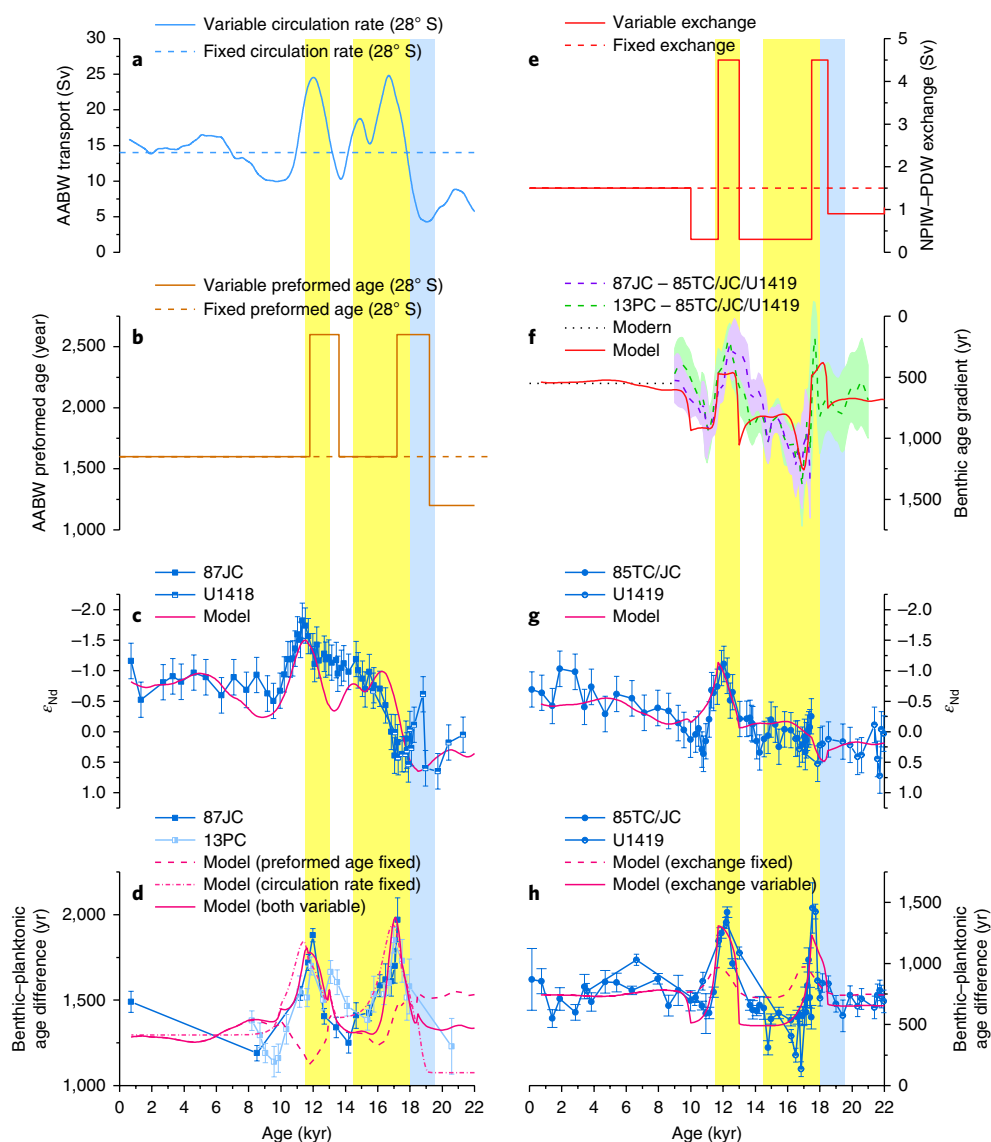


Fig. 3 | Transient simulations of North Pacific circulation tracers. **a**, AABW transport scaled to the rate change of atmospheric CO_2 . **b**, The preformed ^{14}C age of AABW. **c**, Modelled and measured ϵ_{Nd} at deep site EW0408-87JC/U1418. **d**, Modelled and measured benthic-planktonic age differences at deep site EW0408-87JC and W8709A-13PC¹² (Methods). Error bars are 1σ analytical uncertainties. **e**, PDW-NPIW exchange. **f**, Benthic ^{14}C age gradients between NPIW (EW0408-85TC/JC/U1419⁹) and PDW (EW0408-87JC and W8709A-13PC¹²) boxes (95% confidence intervals include uncertainties of both age models and ^{14}C measurements), compared with the model output. The dashed line indicates the modern gradient²⁷. **g, h**, The same as **c** and **d** respectively but for the intermediate-depth site EW0408-85TC/JC/U1419. The standard simulations are plotted using solid lines. Dashed lines indicate model sensitivity tests (Methods). The colour-shaded intervals are the same as in Fig. 2.

the interpretation of North Pacific ϵ_{Nd} in which accelerated abyssal Pacific circulation was driven mainly by Southern Ocean processes.

The intermediate-depth site EW0408-85TC/JC/U1419 recorded relatively constant ϵ_{Nd} from the LGM until about 14 ka, then it covaried with the deep record between 14 and 10 ka (Fig. 2a). In this interval, changes in the intermediate-depth record seemingly precede those of the deep record. This difference in timing can be explained by the shorter transient response time of the smaller intermediate-depth Nd reservoir relative to the deep reservoir (see ‘Transient simulations’ section). Similar modern and LGM ϵ_{Nd} values at intermediate-depth support hypotheses that glacial NPIW circulation was similar to that today²³. Together deep and intermediate-depth records suggest that deglacial acceleration of Pacific circulation and collapse of glacial stratification probably progressed from deep to shallow¹.

Transient simulations

We quantify plausible changes in circulation from these data using a six-box model of the Pacific, starting with modern geostrophic flows well constrained by hydrographic data^{34,35} (Supplementary Fig. 4). We simulate deglacial ϵ_{Nd} and apparent (^{14}C) water-mass age by hypothetically varying AABW transport scaled to Antarctic climate records, and adjust mixing between NPIW and PDW and the preformed age of AABW (Methods, Supplementary Methods). Acknowledging the limitations of box models, we gain quantitative insight into plausible circulation rate changes from these relatively simple perturbations.

The deglacial North Pacific deep ϵ_{Nd} observations are consistent with acceleration of abyssal circulation produced by scaling AABW transport to the rate change of atmospheric CO_2 (Figs. 2c and 3a,c), implying that whatever processes responsible for circulation

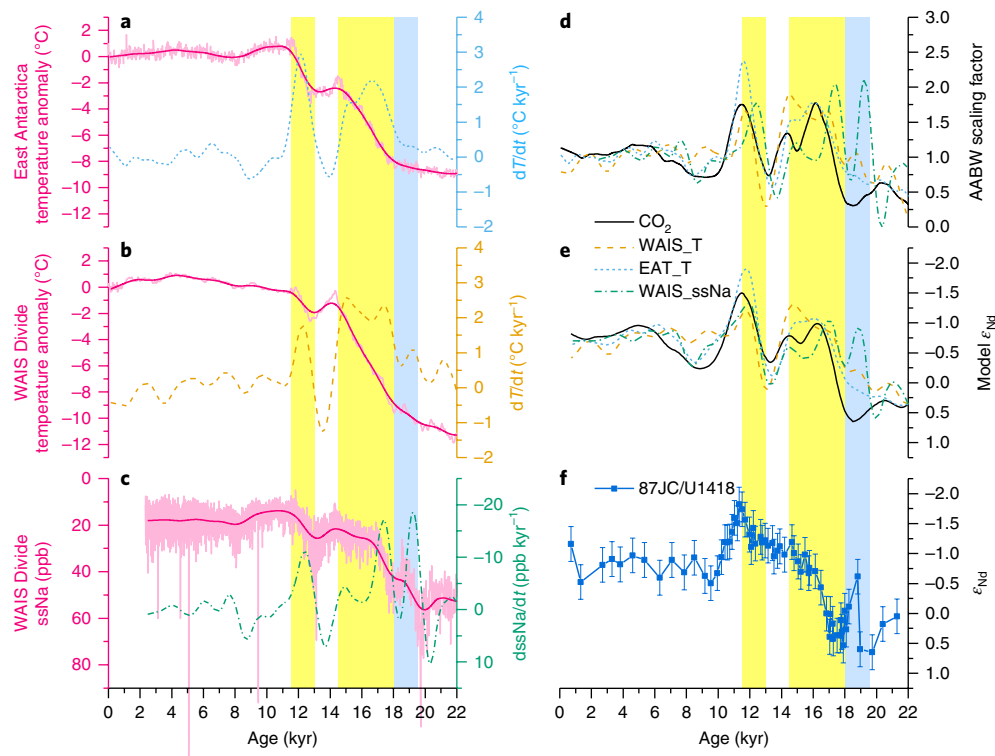


Fig. 4 | Transient simulations using Antarctic climate forcings. **a–c**, The forcings include East Antarctic temperature²⁷ in **a** (EAT_T in **d** and **e**), West Antarctic temperature²⁴ in **b** (WAIS_T in **d** and **e**) and sea ice (sea-salt Na)²⁵ in **c** (WAIS_ssNa in **d** and **e**). We smoothed the original high-resolution records by averaging over 250-year windows and computed the derivatives using non-parametric kernel regression with a bandwidth of 1,000 yr. **d–f**, We then scaled the AABW transport to the z-scores of the derivatives (**d**), which were used to model deep North Pacific ϵ_{Nd} (**e**) and compared with our record (**f**). The scaling is with respect to the modern transport (14 Sv). The simulation reported in Fig. 3c is also shown in **d** and **e** (labelled “CO₂”). The colour-shaded intervals are the same as in Fig. 2.

changes can also plausibly relate to CO₂ changes. Mechanistically, scaling the transport to the rates of Antarctic warming or sea-ice retreat yields similarly reasonable solutions (Fig. 4, Supplementary Methods). For example, the 19 ka ϵ_{Nd} event found at our deep site can be explained if circulation rate is scaled to early sea-ice retreat rate (as documented by ice-core sodium) and warming in West Antarctica. We speculate that this first acceleration of abyssal Pacific circulation, although linked to Antarctic climate events, may have occurred in a heavy-ice-cover regime that was not yet amenable to substantial CO₂ venting.

In our box model, AABW transport into the Pacific changes by a factor of 3, from about 8 Sv (1 Sv = 10⁶ m³ s⁻¹) during the LGM, to about 20–25 Sv during the deglacial intervals of rapidly rising atmospheric CO₂, followed by relaxation to the modern value of about 14 Sv³⁵ (Fig. 3a, Supplementary Fig. 5). By comparing these results with carbon-cycle sensitivities from more comprehensive models, we can estimate plausible impacts of our inferred deglacial abyssal Pacific circulation changes on atmospheric CO₂ and its $\delta^{13}C$. Adopting model sensitivities of 1.5–3.4 ppm Sv^{-136,37} for atmospheric pCO₂ and –0.0069‰ Sv⁻¹³⁸ for atmospheric $\delta^{13}C$ to changes of AABW transport, an approximately 12–17 Sv increase of AABW transport in the early deglaciation could result in about 20–50 ppm increase of pCO₂ and about 0.08–0.12‰ decrease of $\delta^{13}C$. The approximately 9 Sv increase in the late deglaciation could result in about 15–30 ppm increase of pCO₂ and about 0.06‰ decrease of $\delta^{13}C$. These estimates are comparable to the observed stepwise changes of about 50 ppm and about 30 ppm increase of pCO₂ and about 0.3‰ and about 0.1‰ decrease of $\delta^{13}C$ in these intervals^{28,30,31} respectively (Fig. 2c,d), suggesting that acceleration of the abyssal Pacific circulation rate may be

an important, and perhaps dominant, control of deglacial atmospheric CO₂ rise.

In the context of these abyssal circulation rate changes, the intermediate-depth ϵ_{Nd} record can be simulated by varying NPIW–PDW exchange (related to subsurface stratification and mixing), wherein progressively upward destratification started in the early stage of the Antarctic warming intervals (Fig. 3e,g, Supplementary Fig. 5). The strong NPIW–PDW exchange required in the model at about 17.5 ka and about 12.5 ka reflects weaker intermediate-to-deep stratification than today, implying easier access of carbon from the deep-ocean reservoir to the surface and the potential for some CO₂ venting in the North Pacific^{9,39}. Differences in our model transient responses of ϵ_{Nd} and ¹⁴C age in the intermediate and deep boxes to the same physical events (Fig. 3) highlight that tracers with different geochemistries need not respond ‘in phase’ with each other but are fundamentally mediated by tracer residence times at various depths.

Superficially, inferred deglacial acceleration of abyssal Pacific circulation seems to contradict discoveries of ¹⁴C-deficient deep water masses in the North Pacific¹² (Fig. 3d). Our simulations, however, can reproduce the observed apparently ‘old’ deglacial water-mass ages by increasing the preformed ¹⁴C age of southern-source waters at times of increasing AABW transport (Fig. 3b, Supplementary Fig. 6). This increase in preformed ¹⁴C age (by 1,000 yr) would have made the ¹⁴C age (with respect to the atmosphere) of Antarctic surface water approach, but not exceed, that of the deep Pacific, implying efficient mixing of PDW into circumpolar regions¹ and inefficient isotopic gas exchange. In our model, changes of preformed age dominate over that of circulation rate in deep Pacific ¹⁴C records (Fig. 3d).

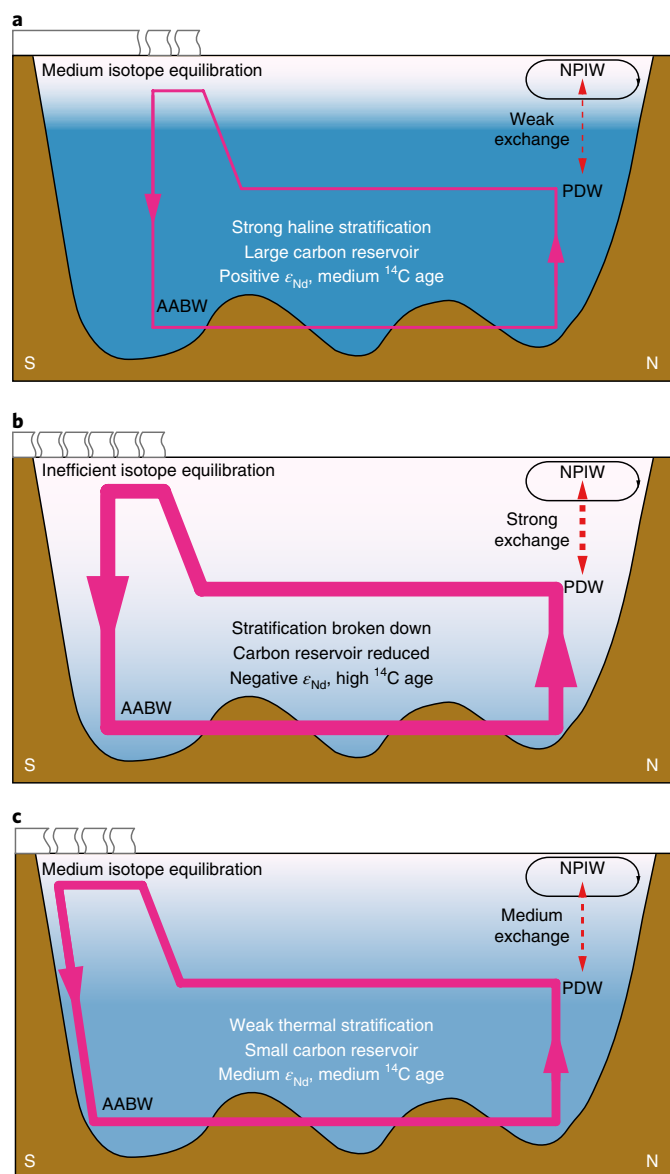


Fig. 5 | Conceptual models of LGM to Holocene circulation evolution in the Pacific. **a**, LGM. Strong haline stratification and sluggish deep circulation. Pacific-wide deep carbon reservoir developed. **b**, Deglacial flushing events. Strong overturning and weak deep stratification. Deep carbon reservoir is released to the atmosphere and reaches intermediate depth. Preformed ages are high. **c**, Modern. Weak thermal stratification, moderate overturning and intermediate preformed ages. The circulation strength is indicated by the thickness of the overturning cell, and the interior stratification is represented using NPIW–PDW exchange (weak exchange is equivalent to stronger stratification) and the gradient of colour shading.

Greater deglacial preformed ^{14}C ages of Southern Ocean water masses may result from weaker stratification and increasing upwelling around Antarctica³². Inefficient carbon isotopic equilibration is reasonable given ice-strewn waters as sea ice retreated and excess CO_2 vented to the atmosphere. Reconstructions of deglacial preformed ^{14}C age in the AABW formation region do not exist yet, but a recent global data synthesis suggests changes of deglacial Southern Ocean surface preformed age are necessary to explain the distribution of benthic ^{14}C in the ocean interior⁴⁰. A subantarctic record¹⁶ (MD07-3076, $44^\circ 4.46' \text{S}$, South Atlantic) shows pronounced increases of surface reservoir age of magnitudes ($\sim 1,000$ yr) and timing similar

to our model prediction. High apparent deglacial reservoir ages were also found in the Eastern Equatorial Pacific⁴¹ and South Pacific¹⁰, implying that redistribution of carbon in shallow subsurface mode waters sourced from the Southern Ocean propagated high preformed ^{14}C age water to lower-latitude upwelling regions where some CO_2 could have vented during the deglaciation⁴².

In the North Pacific, the deep-to-intermediate gradient of benthic ^{14}C reservoir age was smaller than today during our inferred NPIW–PDW mixing events (Fig. 3f), even as apparent ^{14}C water-mass ages at both depths increased (Fig. 3d,h). This too reflects changes in preformed ^{14}C in the interior Pacific: the deep ‘old’ ^{14}C age signal reached intermediate depth as abyssal stratification weakened during the deglaciation.

Alternative hypotheses

Changes in preformed ϵ_{Nd} values in Southern Ocean source waters alone cannot explain our North Pacific data, because, unlike ^{14}C , the effect of preformed properties on deep-sea ϵ_{Nd} is limited^{19–21} (Methods, Supplementary Methods). In our model we prescribe the preformed ϵ_{Nd} using published South Ocean records as boundary conditions (Methods, Supplementary Discussion, Supplementary Fig. 7). The model result therefore accounts for available ϵ_{Nd} data from both the Southern Ocean (dominated by mixing) and North Pacific (dominated by benthic exposure time after the long abyssal transit).

Production of North Pacific intermediate or deep water also cannot explain our North Pacific observations, with the possible exception of a short interval (16–17 ka) when benthic–planktonic age differences became smaller than today at our intermediate-depth site^{7,9,43} (Fig. 3h, Supplementary Discussion). Even in this case benthic ^{14}C precludes a northern-sourced water mass reaching the deep ocean ($>2,700$ m, depth of W8709A-13PC): not only did the deep site benthic–planktonic ^{14}C age differences remain higher than today, but also the deep-to-intermediate-depth benthic ^{14}C gradient increased during this interval (Fig. 3d,f, Supplementary Fig. 8). Thus, if an intermediate water mass formed in the Sea of Okhotsk and Bering Sea (as it does today), its effects were small; the ϵ_{Nd} values provide no evidence for such a water mass in the Northeast Pacific (Supplementary Discussion).

Theoretical arguments suggest that Southern Ocean surface buoyancy forcing can directly regulate stratification in the ocean interior⁴, even in the North Pacific. As such, it is not necessary to invoke local deep-water formation to explain the collapse of intermediate-to-deep stratification suggested by our data and simulations. Rather, the strong correlation between our deep records and Antarctic climate can be readily reconciled if Antarctic forcings were a significant factor controlling the subsurface water-mass properties of the North Pacific.

Finally, the ϵ_{Nd} data are inconsistent with hypotheses that changes of the Atlantic Meridional Overturning Circulation (AMOC) controlled properties of the deep Pacific during the deglaciation (Supplementary Discussion, Supplementary Fig. 7). Reduction of low- ϵ_{Nd} North Atlantic Deep Water should lead to an increase of deep Pacific ϵ_{Nd} ⁴⁴, yet during the intervals of weakest AMOC⁴⁵ (14.5–17.5 ka and 11.5–12.5 ka) both deep North Pacific and Southern Ocean³³ ϵ_{Nd} decreased.

A search for mechanisms and future implications

Our data and model simulations lead to a conceptual understanding of the deep Pacific circulation and the deglacial flushing of its carbon reservoir via abyssal overturning from the south³⁵ (Fig. 5). Although our data do not fully constrain the water-mass transformation processes around Antarctica, they provide key constraints regarding the scale and timing of changes in the abyssal overturning cell and the extent of gas-isotope exchange required to explain the ^{14}C signal in the ocean interior.

A likely candidate mechanism is found in Antarctic sea ice, which controls both buoyancy flux^{4,46} and gas exchange^{14,47}. Most model simulations generate expanded sea ice during glacial times and relate sea-ice area to buoyancy loss and increased abyssal stratification^{4,46}, but the effects of sea ice on gas exchange and isotopic equilibration remain poorly known⁴⁷. During the deglaciation, sea-ice breakup and transport in a divergent wind field during warming events may create a net freshwater export to subpolar latitudes important for water-mass transformation⁴⁸. The intensity and position of Southern Hemisphere westerlies also play roles in northward transport of near-surface waters, southward return flow of PDW to the Antarctic and the upwelling of deep water to the surface³². In addition, accumulation of geothermal heat⁴⁹ may have added buoyancy to the ocean interior due to both sluggish glacial circulation and an increase of deglacial hydrothermal activity⁵⁰. Further exploration of possible mechanisms will be informed by the strong constraint on changing circulation rates provided by our North Pacific ϵ_{Nd} data.

The deglacial changes in abyssal circulation suggested here can be envisioned as a transition from a predominantly haline-stratified glacial mode to a weakly thermal-stratified modern mode^{51,52} (Fig. 5), which probably implies points of instability. This appears to happen in two main steps in the deep Pacific, in both the north (this study) and south¹, coincident with Antarctic warming and CO₂ rise. Steps in the deep Atlantic occurred later during the Bølling–Allerød and early Holocene warming periods⁵³, and are not aligned with CO₂ increase. The abyssal Pacific circulation, forced from the south, is more likely to have tapped the larger deep-ocean carbon reservoir, and appears to be a key to deglacial CO₂ rise.

At present, the deep Pacific still retains a substantial carbon reservoir, and future transfer of carbon from this reservoir to the atmosphere via the Southern Ocean is conceivable. Projections of future circulation have so far focused mainly on changes forced by meltwater in the North Atlantic. Our reconstructions of Pacific overturning in the past motivate additional focus on the Southern Ocean and the Pacific abyssal circulation, for which there is no consensus in models even as to the sign of potential future changes⁵⁴.

Methods

Methods, including statements of data availability and any associated accession codes and references, are available at <https://doi.org/10.1038/s41561-018-0205-6>.

Received: 23 January 2018; Accepted: 13 July 2018;
Published online: 13 August 2018

References

- Sikes, E. L., Allen, K. A. & Lund, D. C. Enhanced $\delta^{13}\text{C}$ and $\delta^{18}\text{O}$ differences between the South Atlantic and South Pacific during the last glaciation: the deep gateway hypothesis. *Paleoceanography* **32**, 1000–1017 (2017).
- Curry, W. B. & Oppo, D. W. Glacial water mass geometry and the distribution of $\delta^{13}\text{C}$ of ΣCO_2 in the western Atlantic Ocean. *Paleoceanography* **20**, PA1017 (2005).
- Wunsch, C. Determining paleoceanographic circulations, with emphasis on the Last Glacial Maximum. *Quat. Sci. Rev.* **22**, 371–385 (2003).
- Jansen, M. F. & Nadeau, L.-P. The effect of Southern Ocean surface buoyancy loss on the deep-ocean circulation and stratification. *J. Phys. Oceanogr.* **46**, 3455–3470 (2016).
- Marchitto, T. M., Lehman, S. J., Ortiz, J. D., Flückiger, J. & van Geen, A. Marine radiocarbon evidence for the mechanism of deglacial atmospheric CO₂ rise. *Science* **316**, 1456–1459 (2007).
- Broecker, W. et al. Radiocarbon age of late glacial deep water from the equatorial Pacific. *Paleoceanography* **22**, PA2206 (2007).
- Okazaki, Y. et al. Deepwater formation in the North Pacific during the Last Glacial Termination. *Science* **329**, 200–204 (2010).
- Burke, A. & Robinson, L. F. The Southern Ocean's role in carbon exchange during the last deglaciation. *Science* **335**, 557–561 (2012).
- Davies-Walczak, M. et al. Late Glacial to Holocene radiocarbon constraints on North Pacific Intermediate Water ventilation and deglacial atmospheric CO₂ sources. *Earth Planet. Sci. Lett.* **397**, 57–66 (2014).
- Rose, K. A. et al. Upper-ocean-to-atmosphere radiocarbon offsets imply fast deglacial carbon dioxide release. *Nature* **466**, 1093–1097 (2010).
- Cook, M. S. & Keigwin, L. D. Radiocarbon profiles of the NW Pacific from the LGM and deglaciation: evaluating ventilation metrics and the effect of uncertain surface reservoir ages. *Paleoceanography* **30**, 174–195 (2015).
- Lund, D. C., Mix, A. C. & Southon, J. Increased ventilation age of the deep northeast Pacific Ocean during the last deglaciation. *Nat. Geosci.* **4**, 771–774 (2011).
- Sikes, E. L., Cook, M. S. & Guilderson, T. P. Reduced deep ocean ventilation in the Southern Pacific Ocean during the last glaciation persisted into the deglaciation. *Earth Planet. Sci. Lett.* **438**, 130–138 (2016).
- Jones, D. C., Ito, T., Takano, Y. & Hsu, W.-C. Spatial and seasonal variability of the air-sea equilibration timescale of carbon dioxide. *Glob. Biogeochem. Cycles* **28**, 1163–1178 (2014).
- Koeve, W., Wagner, H., Kähler, P. & Oschlies, A. ¹⁴C-age tracers in global ocean circulation models. *Geosci. Model Dev.* **8**, 2079–2094 (2015).
- Skinner, L. C., Fallon, S., Waelbroeck, C., Michel, E. & Barker, S. Ventilation of the deep Southern Ocean and deglacial CO₂ rise. *Science* **328**, 1147–1151 (2010).
- Sarnthein, M., Balmer, S., Grootes, P. M. & Mudelsee, M. Planktic and benthic ¹⁴C reservoir ages for three ocean basins, calibrated by a suite of ¹⁴C plateaus in the glacial-to-deglacial Suigetsu atmospheric ¹⁴C record. *Radiocarbon* **57**, 129–151 (2015).
- Lacan, F. & Jeandel, C. Neodymium isotopes as a new tool for quantifying exchange fluxes at the continent–ocean interface. *Earth Planet. Sci. Lett.* **232**, 245–257 (2005).
- Abbott, A. N., Haley, B. A. & McManus, J. Bottoms up: sedimentary control of the deep North Pacific Ocean's ϵ_{Nd} signature. *Geology* **43**, 1035–1035 (2015).
- Du, J., Haley, B. A. & Mix, A. C. Neodymium isotopes in authigenic phases, bottom waters and detrital sediments in the Gulf of Alaska and their implications for paleo-circulation reconstruction. *Geochim. Cosmochim. Acta* **193**, 14–35 (2016).
- Haley, B. A., Du, J., Abbott, A. N. & McManus, J. The impact of benthic processes on rare earth element and neodymium isotope distributions in the oceans. *Front. Mar. Sci.* **4**, 426 (2017).
- Gebbie, G. & Huybers, P. The mean age of ocean waters inferred from radiocarbon observations: sensitivity to surface sources and accounting for mixing histories. *J. Phys. Oceanogr.* **42**, 291–305 (2012).
- Menviel, L. et al. Poorly ventilated deep ocean at the Last Glacial Maximum inferred from carbon isotopes: a data–model comparison study. *Paleoceanography* **32**, 2–17 (2016).
- Cuffey, K. M. et al. Deglacial temperature history of West Antarctica. *Proc. Natl Acad. Sci. USA* **113**, 14249–14254 (2016).
- WAIS Divide Project Members. Onset of deglacial warming in West Antarctica driven by local orbital forcing. *Nature* **500**, 440–444 (2013).
- Clark, P. U., McCabe, A. M., Mix, A. C. & Weaver, A. J. Rapid rise of sea level 19,000 years ago and its global implications. *Science* **304**, 1141–1144 (2004).
- Parrenin, F. et al. Synchronous change of atmospheric CO₂ and Antarctic temperature during the last deglacial warming. *Science* **339**, 1060–1063 (2013).
- Marcott, S. A. et al. Centennial-scale changes in the global carbon cycle during the last deglaciation. *Nature* **514**, 616–619 (2014).
- Bereiter, B., Shackleton, S., Baggenstos, D., Kawamura, K. & Severinghaus, J. Mean global ocean temperatures during the last glacial transition. *Nature* **553**, 39 (2018).
- Schmitt, J. et al. Carbon isotope constraints on the deglacial CO₂ rise from ice cores. *Science* **336**, 711–714 (2012).
- Bauska, T. K. et al. Carbon isotopes characterize rapid changes in atmospheric carbon dioxide during the last deglaciation. *Proc. Natl Acad. Sci. USA* **113**, 3465–3470 (2016).
- Anderson, R. F. et al. Wind-driven upwelling in the Southern Ocean and the deglacial rise in atmospheric CO₂. *Science* **323**, 1443–1448 (2009).
- Basak, C. et al. Breakup of last glacial deep stratification in the South Pacific. *Science* **359**, 900–904 (2018).
- Talley, L. D. Freshwater transport estimates and the global overturning circulation: shallow, deep and throughflow components. *Prog. Oceanogr.* **78**, 257–303 (2008).
- Talley, L. D. Closure of the global overturning circulation through the Indian, Pacific, and Southern Oceans: schematics and transports. *Oceanography* **21**, 80–97 (2013).
- Menviel, L., England, M. H., Meissner, K. J., Mouchet, A. & Yu, J. Atlantic–Pacific seesaw and its role in outgassing CO₂ during Heinrich events. *Paleoceanography* **29**, 58–70 (2014).
- Lauderdale, J. M., Williams, R. G., Munday, D. R. & Marshall, D. P. The impact of Southern Ocean residual upwelling on atmospheric CO₂ on centennial and millennial timescales. *Clim. Dyn.* **48**, 1611–1631 (2017).
- Menviel, L., Mouchet, A., Meissner, K. J., Joos, F. & England, M. H. Impact of oceanic circulation changes on atmospheric $\delta^{13}\text{C}$. *Glob. Biogeochem. Cycles* **29**, 1944–1961 (2015).

39. Gray, W. R. et al. Deglacial upwelling, productivity and CO₂ outgassing in the North Pacific Ocean. *Nat. Geosci.* **11**, 340–344 (2018).
40. Zhao, N., Marchal, O., Keigwin, L., Amrhein, D. & Gebbie, G. A synthesis of deglacial deep-sea radiocarbon records and their (in)consistency with modern ocean ventilation. *Paleoceanogr. Paleoclimatology* **33**, 128–151 (2018).
41. de la Fuente, M., Skinner, L., Calvo, E., Pelejero, C. & Cacho, I. Increased reservoir ages and poorly ventilated deep waters inferred in the glacial Eastern Equatorial Pacific. *Nat. Commun.* **6**, 7420 (2015).
42. Martínez-Boti, M. A. et al. Boron isotope evidence for oceanic carbon dioxide leakage during the last deglaciation. *Nature* **518**, 219–222 (2015).
43. Rae, J. W. B. et al. Deep water formation in the North Pacific and deglacial CO₂ rise. *Paleoceanography* **29**, 645–667 (2014).
44. Friedrich, T., Timmermann, A., Stichel, T. & Pahnke, K. Ocean circulation reconstructions from ϵ_{Nd} : a model-based feasibility study. *Paleoceanography* **29**, 1003–1023 (2014).
45. McManus, J. F., Francois, R., Gherardi, J.-M., Keigwin, L. D. & Brown-Leger, S. Collapse and rapid resumption of Atlantic meridional circulation linked to deglacial climate changes. *Nature* **428**, 834–837 (2004).
46. Marzocchi, A. & Jansen, M. F. Connecting Antarctic sea ice to deep-ocean circulation in modern and glacial climate simulations. *Geophys. Res. Lett.* **44**, 2017GL073936 (2017).
47. Loose, B., McGillis, W. R., Perovich, D., Zappa, C. J. & Schlosser, P. A parameter model of gas exchange for the seasonal sea ice zone. *Ocean Sci* **10**, 17–28 (2014).
48. Abernathy, R. P. et al. Water-mass transformation by sea ice in the upper branch of the Southern Ocean overturning. *Nat. Geosci.* **9**, 596–601 (2016).
49. Adkins, J. F., Ingersoll, A. P. & Pasquero, C. Rapid Climate Change and conditional instability of the glacial deep ocean from the thermobaric effect and geothermal heating. *Quat. Sci. Rev.* **24**, 581–594 (2005).
50. Lund, D. C. et al. Enhanced East Pacific Rise hydrothermal activity during the last two glacial terminations. *Science* **351**, 478–482 (2016).
51. Adkins, J. F., McIntyre, K., & Schrag, D. P. The salinity, temperature, and $\delta^{18}\text{O}$ of the glacial deep ocean. *Science* **298**, 1769–1773 (2002).
52. Zahn, R. & Mix, A. C. Benthic foraminiferal $\delta^{18}\text{O}$ in the ocean's temperature–salinity–density field: constraints on Ice Age thermohaline circulation. *Paleoceanography* **6**, 1–20 (1991).
53. Roberts, J. et al. Evolution of South Atlantic density and chemical stratification across the last deglaciation. *Proc. Natl Acad. Sci. USA* **113**, 514–519 (2016).
54. Meijers, A. J. S. The Southern Ocean in the Coupled Model Intercomparison Project phase 5. *Philos. Trans. R. Soc. A* **372**, 20130296 (2014).
55. Bereiter, B. et al. Revision of the EPICA Dome C CO₂ record from 800 to 600 kyr before present. *Geophys. Res. Lett.* **42**, 542–549 (2015).
56. Böhm, E. et al. Strong and deep Atlantic meridional overturning circulation during the last glacial cycle. *Nature* **517**, 73–76 (2015).
57. Key, R. M. et al. A global ocean carbon climatology: results from Global Data Analysis Project (GLODAP). *Glob. Biogeochem. Cycles* **18**, GB4031 (2004).

Acknowledgements

We thank J. Muratli for assistance with bulk sediment digestion and A. Ungerer for assistance with elemental and isotope analyses at the W. M. Keck Collaboratory for Plasma Spectrometry at Oregon State University. We thank the OSU Marine and Geology Repository and the International Ocean Discover Program for providing sediment samples. IODP-U1418 samples were provided by C. Belanger. This study was supported by NSF grant MGG-1357529 (A.C.M. and B.A.H.).

Author contributions

J.D., B.A.H. and A.C.M. designed this study. J.D. generated neodymium isotope data with assistance from B.A.H. and created the box model with assistance from A.C.M. J.D. wrote the initial manuscript with extensive input from A.C.M. and B.A.H. M.H.W. and S.K.P. assisted with the chronology and the interpretation of radiocarbon data. All authors contributed to the conceptual ideas and provided comments on the manuscript.

Competing interests

The authors declare no competing interests.

Additional information

Supplementary information is available for this paper at <https://doi.org/10.1038/s41561-018-0205-6>.

Reprints and permissions information is available at www.nature.com/reprints.

Correspondence and requests for materials should be addressed to J.D.

Publisher's note: Springer Nature remains neutral with regard to jurisdictional claims in published maps and institutional affiliations.

Methods

Neodymium isotopes. The authigenic ϵ_{Nd} records were generated using the 'HH4' method described previously²⁰, wherein non-decarbonated bulk sediments were reductively leached to extract Nd from authigenic Fe–Mn oxyhydroxides. This method was extensively tested on a large array of core-top and volcanic ash samples to show that it can faithfully extract authigenic components with negligible contamination from lithogenic phases, including volcanic ash²⁰. Decarbonation was abandoned, as it probably leads to lithogenic contamination^{58–63}. The validity of our leaching method is shown using various geochemical tools²⁰ (Supplementary Fig. 3). Untreated sediments for about half of the samples were also digested using a CEM MARS-6 microwave following our published methodology⁶⁴ for analysis of bulk sediment ϵ_{Nd} , which reflects the ϵ_{Nd} of lithogenic sources that dominate the bulk sediment Nd budget.

Nd isotope analysis was done on a Nu Instruments MC-ICP-MS in the W. M. Keck Collaboratory for Plasma Spectrometry at Oregon State University^{19,20}. Mass bias was corrected by normalizing to $^{146}\text{Nd}/^{144}\text{Nd} = 0.7219$ using an exponential law⁶⁵. Samples were bracketed by the JNdi-1 standard⁶⁶ and an in-house standard. Instrumental drift was corrected by normalizing the JNdi-1 analyses to their accepted $^{143}\text{Nd}/^{144}\text{Nd}$ ratio (0.512115⁶⁶). The 2σ $^{143}\text{Nd}/^{144}\text{Nd}$ uncertainty of the JNdi-1 standard was 10 ppm ($n = 278$). The 2σ external uncertainty of the in-house standard was 15 ppm ($n = 274$), that is, $\pm 0.29 \epsilon$ units, which is adopted for uncertainty bars in the figures. Total procedure blanks for Nd isotope analyses of the leachates and digests were $53 \pm 52 \text{ pg}$ ($n = 19$); that is, less than 0.1% of the sample yields. Total sediment digest repeats of two USGS reference materials, AGV-1 and BHVO-2, for the $^{143}\text{Nd}/^{144}\text{Nd}$ ratio were 0.512793 ± 0.000018 (2σ , $n = 10$) and 0.512985 ± 0.000024 (2σ , $n = 9$), both in excellent agreement with published values of 0.512791 ± 0.000013 (2σ) and 0.512984 ± 0.000011 (2σ) respectively⁶⁷.

Radiocarbon and chronology. The age models of EW0408-85TC/JC and EW0408-87JC have been published before and were created using planktonic foraminiferal dates and reservoir ages constrained by tephrochronology and correlation^{9,68,69}. The sample ages are calculated using Bchron⁷⁰ taking into account sample thickness rather than interpolating calibrated ^{14}C dates. Radiocarbon-based age models of U1419 and U1418 are provided by Mix et al. (in preparation) and Walczak et al. (in preparation). The age models of these two sites are created using planktonic ^{14}C dates of exceptionally high density: 71 dates from EW0408-85TC/JC/U1419 and 33 dates from EW0408-87JC/U1418 in the last 22 kyr. Comparison with tephrochronology suggests negligible changes in the surface-ocean reservoir age in this region⁶⁹ and this lends high confidence to our age models. The benthic ^{14}C record of EW0408-85TC/JC was reported previously⁹. Benthic ^{14}C records of EW0408-87JC and U1419 are provided by Praetorius et al. (under review) and Walczak et al. (in preparation) respectively.

The benthic ^{14}C record from core W8709A-13PC (42.1°N, 125.8°W, 2,710 m) on the Gorda Ridge, Northeast Pacific, complements the deep record of EW0408-87JC, which extends only to about 17 ka. During the deglaciation these two records covary (Fig. 3d). Here we use only the new ^{14}C dates from core W8709A-13PC generated at the W. M. Keck Carbon Cycle Accelerator Mass Spectrometry Laboratory at the University of California, Irvine¹². Earlier published data from this core are not included because they came from various laboratories; some of the earlier dates are inconsistent with or have larger uncertainties than the newer high-quality data. The original age model of W8709A-13PC was created using planktonic dates and a reservoir correction of $730 \pm 200 \text{ yr}$ ¹². For internal consistency, we use Bchron⁷⁰ to generate Bayesian age models with both the original reservoir correction and a correction of $870 \pm 80 \text{ yr}$ (that is, $\Delta R = 470 \pm 80 \text{ yr}$) for our Gulf of Alaska cores⁹. The median ages of these two models only differ by about 150 yr (the difference in the reservoir age) and do not affect our interpretations. In the figures we show the age model created using the tephra-calibrated reservoir corrections from the Gulf of Alaska.

The $\epsilon_{\text{Nd}}-^{14}\text{C}$ age twin-tracer approach. The distribution of a tracer in the ocean is controlled not only by circulation (mixing, circulation rate) but also by the preformed properties of the source waters and its interior sources and sinks. In the modern deep Pacific, nearly half of the ^{14}C water-mass age is attributed to preformed age (equivalent to surface reservoir age at the surface ocean), while circulation age (also known as ventilation age, ideal age and so on) accounts for the other half^{5,22}. The strong influence of preformed age reflects inefficient ^{14}C exchange in surface waters around the Antarctic (Supplementary Methods)¹⁴. Benthic ^{14}C age therefore can be used as a tracer of circulation rate only if the preformed age remained constant in the past or is independently known.

Unlike ^{14}C , surficial sources (atmospheric and riverine) are minor in the marine Nd budget^{71–74}, which is dominated by benthic flux from deep-sea (>3,000 m) sediments (Supplementary Methods, Supplementary Fig. 1). Consequently, deep-sea ϵ_{Nd} is sensitive not to its surface preformed properties but to changes in abyssal circulation rate, which controls the exposure time of deep water to benthic flux^{19–21}. The modern Pacific overturning circulation is dominated by the abyssal AABW cell³⁵; it is the densest major water mass in the ocean, and it spreads northward in the Pacific attached to the abyssal seafloor. Consequently, its ϵ_{Nd} is most susceptible to benthic modification²¹, making ϵ_{Nd} an ideal tracer to study the

lower branch of the global overturning circulation. This connection is also strong because water-mass transformation in this lower branch happens mostly along the benthic boundaries due to bottom-enhanced mixing; abyssal circulation in the Pacific thus reflects basin shape, its basic structure is stable^{75–77} and benthic sources of Nd diffuse into the ocean interior efficiently^{19,21}.

In the deep Pacific, the benthic flux has more positive ϵ_{Nd} than the incoming source waters from the Southern Ocean^{19,20}. We therefore expect the water-mass ϵ_{Nd} to become more positive as it ages and its exposure time to the flux increases^{19,20}. This predicted benthic flux effect is demonstrated in the strong correlation between modern core-top authigenic and seawater ϵ_{Nd} and ^{14}C -based circulation age²² (Fig. 1c, Supplementary Fig. 2). Our bottom-up interpretation of authigenic ϵ_{Nd} originates from the improved understanding of marine Nd budget in recent years^{19–21,71–74,78}. An alternative interpretation of authigenic ϵ_{Nd} as a tracer for conservative water-mass mixing assumes that (1) dissolved Nd is predominantly introduced to the ocean at the surface, (2) authigenic phases passively inherit bottom-water ϵ_{Nd} signatures and (3) preformed water-mass end-member ϵ_{Nd} values are time invariant, all of which have been questioned^{18–20,71–74,79–81}. The bottom-up interpretation explains the distributions of not only bottom-water ϵ_{Nd} , but also that of authigenic phases^{19–21,71,78}. Under this framework the authigenic and bottom-water ϵ_{Nd} need not be the same, as seen in the consistent offset between them in the Pacific (Supplementary Fig. 2).

In our $\epsilon_{\text{Nd}}-^{14}\text{C}$ age twin-tracer approach, deep-ocean ϵ_{Nd} is used to constrain abyssal circulation rate because of its high sensitivity to this parameter. The inferred circulation rate information is then used to isolate the preformed-age component of the deep-ocean ^{14}C . In doing so, we also test whether the observed changes in deep ϵ_{Nd} and ^{14}C age were caused by far-field (Southern Ocean) or local (North Pacific) factors. This test is aided by also considering the intermediate-depth ϵ_{Nd} and ^{14}C age, the changes of which are caused by either variations in local intermediate/deep-water formation or mixing with the deep ocean. Overall, we seek a physical explanation of deglacial Pacific circulation (circulation rate and mixing) that is consistent with ϵ_{Nd} and ^{14}C age at both intermediate and deep sites in the North Pacific.

Box model. Our twin-tracer approach is quantified by transiently modelling these two tracers in the Pacific during the deglaciation using a six-box model. Transient modelling is necessary as neither circulation nor tracer distributions are expected to be under steady state during the deglaciation considering the abrupt climate changes. The model was based on the box inverse model of Talley^{34,35,82}, wherein zonal averages of meridional transports at different density layers across 28°S and 24°N were computed using hydrographic data. We merged the density layers into six boxes and defined these boxes with depth. The configuration of these boxes is presented in Supplementary Figure 4. The governing equation of ϵ_{Nd} in each box is (Supplementary Methods)

$$\frac{d\epsilon_{\text{Nd}}}{dt} = \frac{1}{\tau_{\text{Nd}}} \epsilon_{\text{Nd}}^{\text{B}} + \frac{1}{\tau_{\text{w}}} \sum m^i \epsilon_{\text{Nd}}^i - \left(\frac{1}{\tau_{\text{Nd}}} + \frac{1}{\tau_{\text{w}}} \right) \epsilon_{\text{Nd}} \quad (1)$$

where τ_{w} and τ_{Nd} are the residence times of water (with respect to water-mass transport) and Nd (with respect to benthic flux) in the box respectively, $\epsilon_{\text{Nd}}^{\text{B}}$ is the isotope composition of the benthic source and m^i and ϵ_{Nd}^i are the concentration-weighted mixing ratio and isotope composition of the i th source water of the box, representing the conservative mixing of the preformed values. In the box model context, local water residence time is equivalent to benthic exposure time¹⁹ and circulation age²². Here we have ignored surficial (atmospheric and riverine) sources of Nd as they are negligible in the Pacific Nd budget (Supplementary Methods).

At steady state, $\epsilon_{\text{Nd}} = \frac{\tau_{\text{w}}}{\tau_{\text{Nd}} + \tau_{\text{w}}} \epsilon_{\text{Nd}}^{\text{B}} + \frac{\tau_{\text{Nd}}}{\tau_{\text{Nd}} + \tau_{\text{w}}} \sum m^i \epsilon_{\text{Nd}}^i$, that is, ϵ_{Nd} of the box is equal to the weighted average of the benthic source (non-conservative) and preformed (conservative) terms, and the weighing factor is controlled by the ratio $\tau_{\text{w}}/\tau_{\text{Nd}}$. This means that the expression of the benthic source is modulated by the circulation rate, which controls τ_{w} , assuming that τ_{Nd} is constant as we expect during the deglaciation (Supplementary Methods). In the Pacific, τ_{Nd} (~400 yr, Supplementary Methods) is much shorter than τ_{w} (~1,000 yr)^{15,22}, and consequently the benthic source term dominates, explaining the strong correlation between circulation age and ϵ_{Nd} (Fig. 1c, Supplementary Fig. 2a). This contrasts with the modern North Atlantic, where τ_{Nd} is longer than τ_{w} (~200 yr)^{15,22} and where the major deep water mass, North Atlantic Deep Water, is largely isolated from abyssal seafloor by the underlying AABW, leading to quasi-conservative behaviours of ϵ_{Nd} ^{21,83}. The dominance of the benthic flux does not negate the considerable contribution of preformed component to the Pacific Nd budget, and our interpretation of ϵ_{Nd} therefore rests on the interplay of these two components, which is mediated by circulation rate (Supplementary Methods).

Because of the differences between authigenic and bottom-water ϵ_{Nd} (Supplementary Fig. 2b) and between regional and box mean seawater ϵ_{Nd} , authigenic ϵ_{Nd} from an individual site may be offset from the box mean seawater ϵ_{Nd} . Based on our previous survey of the authigenic and seawater ϵ_{Nd} in the Gulf of Alaska²⁰, we adopt an empirical constant that the authigenic ϵ_{Nd} values at our two sites are both +2.8 ϵ higher than the mean seawater ϵ_{Nd} of the NPIW and PDW boxes. Therefore, simulated seawater results are converted to equivalent authigenic ϵ_{Nd} using this constant offset. We note that our interpretations, and the model we

generate, rely only on relative changes in ϵ_{Nd} . The model can be run with either constant (default) or dynamic Nd concentrations (Supplementary Methods).

In modelling water-mass ^{14}C age, we follow the approach of decomposing it to preformed and circulation age components^{15,22} (Supplementary Methods). The governing equation of the water-mass age a in each box is

$$\frac{da}{dt} = \frac{1}{\tau_w} \sum m^i a^i + 1 - \frac{1}{\tau_w} a \quad (2)$$

where m^i and a^i are the mixing ratio and age of the i th source water of the box, representing conservative mixing of the preformed ages; the term '1' indicates aging of the water mass by 1 unit of time per unit time step, that is, the interior source term. At steady state $a = \sum m^i a^i + \tau_w$. Unlike ϵ_{Nd} , the preformed and the circulation age terms are equally weighted, that is, the water-mass age is sensitive to both components. This leads to the possibility that the observed changes in apparent water-mass ^{14}C age may not reflect changes in circulation rate alone.

The differences between the modelled water-mass ages of the NPIW and PDW boxes and the North Pacific surface reservoir age can be directly compared with the benthic–planktonic ^{14}C age differences in our records. Here we assume little or no change in the surface–ocean reservoir age at our North Pacific sites. Based on correlation and tephrochronology, near-surface reservoir ages are constrained to be relatively constant (within a few hundred years) in this region during the deglacial interval^{69,84}.

The model is first configured to describe modern distributions of ϵ_{Nd} and watermass age in the Pacific (Supplementary Methods). We estimated benthic sources and sinks in each box using modern observations of seawater and authigenic ϵ_{Nd} . In the model the seafloor area, including that from the continental shelf and slope and the abyssal plain, exposed in each box is estimated using hypsometric curves⁸⁵ (Supplementary Methods, Supplementary Fig. 1 and Supplementary Table 2).

Transient simulations. In our simulations we assume that benthic flux is constant, which is equivalent to assuming that τ_{Nd} is constant (Supplementary Methods). Our estimates show that the Pacific Nd budget is dominated by benthic flux from deep-sea sediments (>3,000 m) because most of the seafloor area is concentrated below this depth (Supplementary Methods, Supplementary Fig. 1). This suggests that the basal benthic flux should be stable on the timescale of glacial–interglacial cycles, as large-scale deep-sea sediment provenance is primarily controlled by tectonic activities operating on much longer timescales^{86–88}. We further show in the Supplementary Methods that deglacial changes in surficial fluxes of Nd (dust and freshwater/meltwater fluxes) do not significantly affect the Pacific Nd budget, and benthic flux is also not sensitive to sediment redox state (Supplementary Fig. 1) or sedimentation rate. Instead, changes in Southern Ocean water-mass transport are the most likely candidate to explain our ϵ_{Nd} records.

Under this framework, the ϵ_{Nd} and water-mass age of the North Pacific boxes will change in response to forcings specified on the deep Southern Ocean boundary (controlling the influx of Southern Ocean deep waters), the North Pacific surface boundary (controlling local formation of intermediate and potentially deep water) and the NPIW–PDW boundary (controlling vertical mixing) (Supplementary Fig. 4). All the parameters associated with the AAIW box are fixed, as they have limited effect on the North Pacific boxes.

In the deglacial simulations reported in Fig. 3 we identify three adjustable parameters: the scaling factor applied to the transports associated with AABW, that is, F2, F3 and F4 (Supplementary Fig. 4), the scaling factor applied to the PDW–NPIW exchange flux, that is, F6, and the preformed-age anomaly of AABW specified at the southern boundary. We multiply the water fluxes by their respective scaling factors in model simulations. The preformed-age anomaly is assumed to be the same at the 28°S boundary as in the AABW surface formation region, and the implemented preformed-age boundary condition is the modern boundary condition of 1,600 yr plus this anomaly (Supplementary Methods). In these simulations Nd concentrations in each box are fixed. The ϵ_{Nd} values at the southern boundaries are specified based on palaeo-reconstructions in the South Pacific^{33,89–92}: preformed ϵ_{Nd} values of AABW and AAIW are 1.8 ϵ and 1 ϵ higher respectively in the LGM and then decrease to their modern values linearly from 17.5 to 11 ka (Supplementary Methods, Supplementary Fig. 7).

We first carried out LGM steady-state simulations to generate initial values for the deglacial transient simulations. In the sensitivity tests described later (Supplementary Discussion), we adjusted the three parameters to fit the LGM solution to our observations. The chosen parameters are a scaling factor of 0.55 applied to the AABW transports, a scaling factor of 0.6 applied to PDW–NPIW exchange and an AABW preformed age anomaly of –400 yr (Supplementary Figs. 5, 6).

In the deglacial transient simulations, we first adjusted the AABW transport, which was scaled to the rate change of atmospheric CO_2 , to explain our deep North Pacific ϵ_{Nd} record. The rationale is that if changes in AABW transport can explain changes of atmospheric CO_2 then they should also explain our ϵ_{Nd} record. We then adjusted the preformed age of AABW such that together with the inferred AABW transport the deep water-mass age record was explained. Next, we adjusted the NPIW–PDW exchange flux to explain the intermediate-depth benthic age record.

Once these parameters are specified, modelled intermediate-depth ϵ_{Nd} should also fit our observation if our physical explanation is valid, and this serves as an independent check on the model. The deglacial time series of these parameters and model results are shown in Fig. 3. In these simulations we did not seek exact fits to our data but aimed to explain the main events. Therefore, we used simple square-wave schemes for the preformed age of AABW and NPIW–PDW mixing parameters. The simulations that best represent our data are called 'standard simulations' and are plotted using solid lines in Fig. 3.

Sensitivity tests. In Fig. 3 we also show a few model sensitivity tests that are indicated using dashed lines. In Fig. 3d we show experiments with fixed preformed age and fixed circulation rate, that is, constant AABW preformed age and transport respectively. In Fig. 3h we show an experiment with fixed NPIW–PDW exchange. These tests differ from the standard simulation in that only the tested parameters were changed. To run these tests, LGM steady-state solutions were first found that also differ from the standard case only in the tested parameters. Extra simulations in which we scaled the AABW transport to other Antarctic forcings are reported in Fig. 4 (Supplementary Discussion). These simulations are the same as the standard simulations except for the scaling factor applied to AABW transport.

In the Supplementary Discussion we also use sensitivity tests to (1) find the optimal combination of the parameters for the LGM steady-state solution that was used to initialize the deglacial transient simulations (Supplementary Fig. 5), (2) show that the uncertainty in the preformed age of AABW during the LGM does not affect our deglacial transient simulations (Supplementary Fig. 6), (3) show that our deep North Pacific ϵ_{Nd} record cannot be explained by changes in the preformed ϵ_{Nd} of AABW that might be related to changes in North Atlantic Deep Water formation (Supplementary Fig. 7), (3) show that our data are inconsistent with enhanced formation of NPIW or formation of local deep water in the subpolar Northeast Pacific (with the exception of the short interval 16–17 ka), even when plausible changes of the North Pacific surface preformed ϵ_{Nd} and age are considered (Supplementary Fig. 9), and (4) show that fixing Nd concentrations or simulating them dynamically has little influence on the simulated ϵ_{Nd} (Supplementary Fig. 10).

Data availability. The authors declare that the data supporting the findings of this study are available within the article and its supplementary information files. Data are also available on Pangaea (<https://pangaea.de/>) and Paleoclimate Data at NOAA National Centers for Environmental Information (<https://www.ncdc.noaa.gov/data-access/paleoclimatology-data>).

Code availability. The computer codes for the box model and transient simulations are available upon request from the corresponding author.

References

- Howe, J. N. W. et al. Antarctic intermediate water circulation in the South Atlantic over the past 25,000 years. *Paleoceanography* **31**, 1302–1314 (2016).
- Wilson, D. J., Piotrowski, A. M., Galy, A. & Clegg, J. A. Reactivity of neodymium carriers in deep sea sediments: implications for boundary exchange and paleoceanography. *Geochim. Cosmochim. Acta* **109**, 197–221 (2013).
- Blaser, P. et al. Extracting foraminiferal seawater Nd isotope signatures from bulk deep sea sediment by chemical leaching. *Chem. Geol.* **439**, 189–204 (2016).
- Molina-Kescher, M., Frank, M. & Hathorne, E. Nd and Sr isotope compositions of different phases of surface sediments in the South Pacific: extraction of seawater signatures, boundary exchange, and detrital/dust provenance. *Geochem. Geophys. Geosystems* **15**, 3502–3520 (2014).
- Wu, Q. et al. Neodymium isotopic composition in foraminifera and authigenic phases of the South China Sea sediments: implications for the hydrology of the North Pacific Ocean over the past 25 kyr. *Geochem. Geophys. Geosystems* **16**, 3883–3904 (2015).
- Tachikawa, K. et al. The large-scale evolution of neodymium isotopic composition in the global modern and Holocene ocean revealed from seawater and archive data. *Chem. Geol.* **457**, 131–148 (2017).
- Muratli, J. M., McManus, J., Mix, A. & Chase, Z. Dissolution of fluoride complexes following microwave-assisted hydrofluoric acid digestion of marine sediments. *Talanta* **89**, 195–200 (2012).
- O'Nions, R. K., Carter, S. R., Evensen, N. M. & Hamilton, P. J. Geochemical and cosmochemical applications of Nd isotope analysis. *Annu. Rev. Earth Planet. Sci.* **7**, 11–38 (1979).
- Tanaka, T. et al. JNd-1: a neodymium isotopic reference in consistency with LaJolla neodymium. *Chem. Geol.* **168**, 279–281 (2000).
- Weis, D. et al. High-precision isotopic characterization of USGS reference materials by TIMS and MC-ICP-MS. *Geochem. Geophys. Geosystems* **7**, Q08006 (2006).
- Praetorius, S. K. et al. North Pacific deglacial hypoxic events linked to abrupt ocean warming. *Nature* **527**, 362–366 (2015).
- Praetorius, S. K. & Mix, A. C. Synchronization of North Pacific and Greenland climates preceded abrupt deglacial warming. *Science* **345**, 444–448 (2014).

70. Haslett, J. & Parnell, A. A simple monotone process with application to radiocarbon-dated depth chronologies. *J. R. Stat. Soc. Ser. C Appl. Stat.* **57**, 399–418 (2008).
71. Abbott, A. N., Haley, B. A., McManus, J. & Reimers, C. E. The sedimentary flux of dissolved rare earth elements to the ocean. *Geochim. Cosmochim. Acta* **154**, 186–200 (2015).
72. Tachikawa, K., Athias, V. & Jeandel, C. Neodymium budget in the modern ocean and paleo-oceanographic implications. *J. Geophys. Res. Oceans* **108**, 3254 (2003).
73. Arsouze, T., Dutay, J.-C., Lacan, F. & Jeandel, C. Reconstructing the Nd oceanic cycle using a coupled dynamical–biogeochemical model. *Biogeosciences* **6**, 2829–2846 (2009).
74. Rempfer, J., Stocker, T. F., Joos, F., Dutay, J.-C. & Siddall, M. Modelling Nd-isotopes with a coarse resolution ocean circulation model: sensitivities to model parameters and source/sink distributions. *Geochim. Cosmochim. Acta* **75**, 5927–5950 (2011).
75. de Lavergne, C., Madec, G., Roquet, F., Holmes, R. M. & McDougall, T. J. Abyssal ocean overturning shaped by seafloor distribution. *Nature* **551**, 181–186 (2017).
76. Ferrari, R., Mashayek, A., McDougall, T. J., Nikurashin, M. & Campin, J.-M. Turning ocean mixing upside down. *J. Phys. Oceanogr.* **46**, 2239–2261 (2016).
77. de Lavergne, C., Madec, G., Le Sommer, J., Nurser, A. J. G. & Naveira Garabato, A. C. On the consumption of Antarctic Bottom Water in the abyssal ocean. *J. Phys. Oceanogr.* **46**, 635–661 (2015).
78. Abbott, A. N., Haley, B. A. & McManus, J. The impact of sedimentary coatings on the diagenetic Nd flux. *Earth Planet. Sci. Lett.* **449**, 217–227 (2016).
79. Jones, K. M., Khatiwala, S. P., Goldstein, S. L., Hemming, S. R. & van de Flierdt, T. Modeling the distribution of Nd isotopes in the oceans using an ocean general circulation model. *Earth Planet. Sci. Lett.* **272**, 610–619 (2008).
80. Howe, J. N. W., Piotrowski, A. M. & Rennie, V. C. F. Abyssal origin for the early Holocene pulse of unradiogenic neodymium isotopes in Atlantic seawater. *Geology* **44**, 831–834 (2016).
81. Roberts, N. L. & Piotrowski, A. M. Radiogenic Nd isotope labeling of the northern NE Atlantic during MIS 2. *Earth Planet. Sci. Lett.* **423**, 125–133 (2015).
82. Talley, L. D. Shallow, intermediate, and deep overturning components of the global heat budget. *J. Phys. Oceanogr.* **33**, 530–560 (2003).
83. Lambelet, M. et al. Neodymium isotopic composition and concentration in the western North Atlantic Ocean: results from the GEOTRACES GA02 section. *Geochim. Cosmochim. Acta* **177**, 1–29 (2016).
84. Praetorius, S. et al. Interaction between climate, volcanism, and isostatic rebound in Southeast Alaska during the last deglaciation. *Earth Planet. Sci. Lett.* **452**, 79–89 (2016).
85. Menard, H. W. & Smith, S. M. Hypsometry of ocean basin provinces. *J. Geophys. Res.* **71**, 4305–4325 (1966).
86. McLennan, S. M., Hemming, S., McDaniel, D. K. & Hanson, G. N. Geochemical approaches to sedimentation, provenance, and tectonics. *Geol. Soc. Am. Spec. Pap.* **284**, 21–40 (1993).
87. Ziegler, C. L., Murray, R. W., Hovan, S. A. & Rea, D. K. Resolving eolian, volcanogenic, and authigenic components in pelagic sediment from the Pacific Ocean. *Earth Planet. Sci. Lett.* **254**, 416–432 (2007).
88. Dunlea, A. G. et al. Dust, volcanic ash, and the evolution of the South Pacific Gyre through the Cenozoic. *Paleoceanography* **30**, 1078–1099 (2015).
89. Hu, R. et al. Neodymium isotopic evidence for linked changes in Southeast Atlantic and Southwest Pacific circulation over the last 200 kyr. *Earth Planet. Sci. Lett.* **455**, 106–114 (2016).
90. Noble, T. L., Piotrowski, A. M. & McCave, I. N. Neodymium isotopic composition of intermediate and deep waters in the glacial southwest Pacific. *Earth Planet. Sci. Lett.* **384**, 27–36 (2013).
91. Elderfield, H. et al. Evolution of ocean temperature and ice volume through the Mid-Pleistocene Climate Transition. *Science* **337**, 704–709 (2012).
92. Molina-Kescher, M. et al. Reduced admixture of North Atlantic Deep Water to the deep central South Pacific during the last two glacial periods. *Paleoceanography* **31**, 651–668 (2016).